npj | Quantum Materials

www.nature.com/npjquantmats

ARTICLE OPEN

Nematic pairing from orbital-selective spin fluctuations in FeSe

Lara Benfatto[1], Belén Valenzuela[2] and Laura Fanfarillo[3]

FeSe is an intriguing iron-based superconductor. It presents an unusual nematic state without magnetism and can be tuned to increase the critical superconducting temperature. Recently it has been observed a noteworthy anisotropy of the superconducting gaps. Its explanation is intimately related to the understanding of the nematic transition itself. Here, we show that the spin-nematic scenario driven by orbital-selective spin fluctuations provides a simple scheme to understand both phenomena. The pairing mediated by anisotropic spin modes is not only orbital selective but also nematic, leading to stronger pair scattering across the hole and X electron pocket. The delicate balance between orbital ordering and nematic pairing points also to a marked k_z dependence of the hole–gap anisotropy.

npj Quantum Materials (2018)3:56 ; doi:10.1038/s41535-018-0129-9

INTRODUCTION

Soon after the discovery of superconductivity in iron-based systems, it has been proposed that pairing could be unconventional, i.e., based on a non-phononic mechanism.[1,2] This proposal has been triggered, from one side, by the small estimated value of the electron–phonon coupling, and, from the other side, by the proximity in the temperature-doping phase diagram of a magnetic instability nearby the superconducting (SC) one. Within an itinerant-electron picture pairing could be provided by repulsive spin fluctuations (SF) between hole and electron pockets, connected by the same wavevector characteristic of the spin modulations in the magnetic phase (see Fig. 1). This suggestion has been supported and confirmed by an extensive theoretical work, aimed from one side to establish why inter-pockets repulsion can overcome the intra-pocket one[3] and from the other side to provide a quantitative estimate of the SC properties starting from the Random Phase Approximation (RPA)-based description of the SF susceptibility.[4,5]

The success of the itinerant scenario as a unified description of Fe-based materials has been partly questioned by the discovery of superconductivity in the FeSe system. Recent experiments[6–10] detected sizeable SF in FeSe, however, a magnetic phase appears only upon doping. Superconductivity emerges below $T_c \sim 9$ K from the so-called nematic phase.[11] Here at temperatures below $T_S = 90$ K, the anisotropy of the electronic properties is far larger than what expected across a standard tetragonal-to-orthorhombic transition, suggesting that it is driven by electronic degrees of freedom.[11,12] In particular, Angle-Resolved Photoemission Spectroscopy (ARPES) experiments clearly show a dramatic change of the Fermi surface (FS) across T_S, that can be reproduced with an effective crystal-field splitting of the various orbitals.[13–21]

In this situation, the explanation of the observed anisotropy of the SC gaps in FeSe becomes intimately related to the understanding of the nematic transition itself. Extensive experimental studies on the FeSe-based material, ranging from quasiparticle interference imaging[22,23] and ARPES measurements,[24–28] to thermal probes,[29,30] suggest that the SC gap in FeSe is highly anisotropic on both hole and electron pockets. By defining θ the angle formed with the k_x axis measured with respect to the center of each pocket, one finds that the gap is larger at $\theta = 0$ on the Γ pocket, where the predominant character in the nematic phase is xz,[19,26,27] and at $\theta = \pi/2$ on the X pocket, where the dominant character is yz, Fig. 1b. Thus, accounting for an orbital-dependent SC order parameter does not reproduce the observed gap hierarchy, and additional phenomenological modifications of the pairing mechanism must be introduced[22,26,31] to describe the experiments.

Among the various attempts to theoretically understand the nematic phase from microscopic models, we have recently emphasized the outcomes of a theoretical approach which correctly incorporates the feedback between orbital degrees of freedom and SF.[19,32,33] From one side, the degree of orbital nesting between hole and electron pockets is crucial to determine the temperature scale where SF beyond RPA drive the spin-nematic instability,[32] making SF at $\mathbf{Q}_X = (\pi/a, 0)$ and $\mathbf{Q}_Y = (0, \pi/a)$ anisotropic below T_S.[34] From the other side, SF renormalize the quasiparticle dispersion, so that the orbital ordering observed below T_S is a consequence of the spin nematicity, thanks to an orbital-selective shrinking mechanism.[19] In this work, we show that such orbital-selective spin fluctuations (OSSF) provide also the key pairing mechanism needed to understand the SC properties of FeSe. Within an orbital-selective spin-nematic scenario, the C_4 symmetry breaking of the SF below T_S provides a pairing mechanism that is not only orbital selective but also nematic, in the sense that inter-pocket pair scattering along the ΓX and ΓY directions becomes anisotropic. As we show below, accounting only for the nematic band-structure reconstruction of the FS, the SC gap of the Γ pocket follows the modulation of the dominant xz orbital, with a weak relative maximum at $\theta = \pi/2$, in striking disagreement with the experiments. The nematic pairing provided

[1]ISC-CNR, Department of Physics, "Sapienza" University of Rome, P.le A. Moro 5, 00185 Rome, Italy; [2]Materials Science Factory, Instituto de Ciencia de Materiales de Madrid, ICMM-CSIC, Cantoblanco, E-28049 Madrid, Spain and [3]CNR-IOM, International School for Advanced Studies (SISSA), Via Bonomea 265, I-34136 Trieste, Italy
Correspondence: Laura Fanfarillo (laura.fanfarillo@sissa.it)

Received: 9 May 2018 Accepted: 15 October 2018
Published online: 02 November 2018

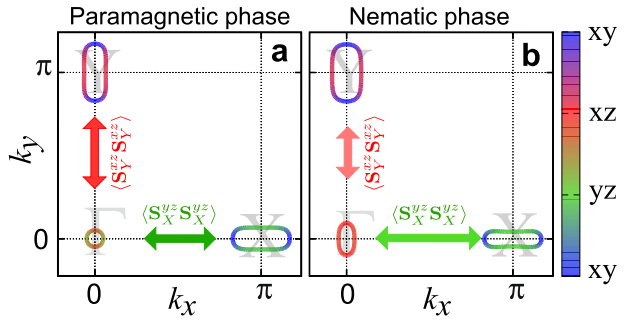

Fig. 1 FeSe Fermi surfaces at $k_z = 0$. **a** Paramagnetic phase. **b** Nematic phase. The colors represent the main orbital character of the Fermi surface. The green/red arrows denote the orbital-selective spin fluctuations (OSSF), connecting hole and electron pockets at different momenta, see Eqs. (6) and (7). The spin fluctuations along ΓX and ΓY are equivalent in the paramagnetic phase **a** and become anisotropic in the nematic one **b**

by OSSF is crucial to enhance the *yz* component of the SC order parameter, explaining why the anisotropy of the SC gap at Γ follows the subdominant *yz* orbital character of the underlying FS.[26,27] We also discuss its implications for the gap-structure measured at $k_z = \pi$ (refs. [24,25,28]), where hole pocket retains a larger *yz* character even in the nematic phase, making the nematic pairing responsible for an enhancement of the moderate gap anisotropy triggered already by orbital-ordering effects.[35]

RESULTS

Model

To compute the SC properties of FeSe, we start from a low-energy model adapted from ref. [36]. The orbital content of each pocket is encoded via a rotation from the fermionic operators c_{xz}, c_{yz}, c_{xy} in the orbital basis to the ones describing the outer hole pocket (*h*) at Γ and the electronic pockets at *X* (e_X) and at *Y* (e_Y):

$$h_{\mathbf{k}} = u_{\Gamma,\mathbf{k}} c_{yz,\mathbf{k}} - v_{\Gamma,\mathbf{k}} c_{xz,\mathbf{k}}, \tag{1}$$

$$e_{X,\mathbf{k}} = u_{X,\mathbf{k}} c_{yz,\mathbf{k}} - i v_{X,\mathbf{k}} c_{xy,\mathbf{k}}, \tag{2}$$

$$e_{Y,\mathbf{k}} = u_{Y,\mathbf{k}} c_{xz,\mathbf{k}} - i v_{Y,\mathbf{k}} c_{xy,\mathbf{k}}, \tag{3}$$

where the explicit definition of the coefficients $u_{\ell,\mathbf{k}}, v_{\ell,\mathbf{k}}$ with $\ell = \Gamma, X, Y$ is given in Supplementary Note 1. For example, for the hole pocket in the tetragonal phase $u_{\Gamma,\mathbf{k}_F} \sim \cos\theta$ and $v_{\Gamma,k_F} \sim \sin\theta$, accounting for the predominant orbital character of the FS represented in Fig. 1a. By using the identities (1)–(3), one can establish[32,37] (see also Supplementary Note 2) a precise correspondence between the orbital character of the spin operator and the momenta $\mathbf{Q}_X$ or $\mathbf{Q}_Y$ connecting the hole and the *X*/*Y* pockets:

$$\mathbf{S}(\mathbf{Q}_X) \equiv \mathbf{S}_X^{yz} = \sum_{\mathbf{k}} u_{\Gamma,\mathbf{k}} h_{\mathbf{k}}^{\dagger} \vec{\sigma} u_{X,\mathbf{k}+\mathbf{Q}_X} e_{X,\mathbf{k}+\mathbf{Q}_X}, \tag{4}$$

$$\mathbf{S}(\mathbf{Q}_Y) \equiv \mathbf{S}_Y^{xz} = \sum_{\mathbf{k}} -v_{\Gamma,\mathbf{k}} h_{\mathbf{k}}^{\dagger} \vec{\sigma} u_{Y,\mathbf{k}+\mathbf{Q}_Y} e_{Y,\mathbf{k}+\mathbf{Q}_Y}. \tag{5}$$

Since *xz* states are absent at *X* the $S_{\mathbf{q}}^{xz}$ operator has no component at the wavevector $\mathbf{Q}_X$ connecting the Γ and *X* pocket, and vice versa for the *yz* states. This leads to OSSF at different momenta, as depicted in Fig. 1:

$$\langle \mathbf{S} \cdot \mathbf{S} \rangle(\mathbf{Q}_X) \Rightarrow \langle \mathbf{S}_X^{yz} \cdot \mathbf{S}_X^{yz} \rangle, \tag{6}$$

$$\langle \mathbf{S} \cdot \mathbf{S} \rangle(\mathbf{Q}_Y) \Rightarrow \langle \mathbf{S}_Y^{xz} \cdot \mathbf{S}_Y^{xz} \rangle. \tag{7}$$

The existence of OSSF provides a natural explanation of the orbital ordering observed in the nematic phase of FeSe. In fact, the self-energy corrections due to spin exchange imply a shift in the chemical potential with opposite sign for the hole and electron pockets, leading in both cases to a shrinking of the FS[19,38] that explains why experimentally they are always smaller than LDA predictions.[19,39,40] Within the OSSF model, due to the orbital-selective nature of SF, this mechanism is also orbital-dependent.[19] As a consequence, within a spin-nematic scenario, the C_4 symmetry breaking of SF along Γ*X* and Γ*Y* explains also the orbital ordering observed in the nematic phase. It has been shown[19] that, by assuming stronger SF at $\mathbf{Q}_X$ below T_S, the self-energy difference ΔΣ between the *xz* and *yz* orbitals induces an orbital splitting being positive at Γ and negative at the electron pockets, leading to the observed deformations of the FS below T_S.[11,15,17,19–21] Even though this orbital-selective shrinking mechanism is generic, its effect can be quantitatively different in the various family of iron-based superconductors. For example, in the 122 family the survival of the inner hole pocket enhances the degree of orbital nesting between hole and electron pockets favoring magnetism, this explains why in 122 the nematic transition is immediately followed by the magnetic one.[32] The quantitative determination of the nematic splitting induced by the nematic spin modes requires a direct comparison with the low-energy band dispersion, as done explicitly for FeSe in ref. [19]. Here, we take these results for granted and we start from a low-energy model that includes already the effective masses, isotropic shrinking, and nematic splittings needed to reproduce the ARPES FS measured in the nematic phase above T_c, and the k_z dependence of the hole pocket between the Γ ($k_z = 0$) and Z ($k_z = \pi$) point (see Supplementary Note 3). The resulting FS at $k_z = 0$ is shown in Fig. 1.

The effect of the nematic orbital splitting on the orbital factors below T_S is shown in Fig. 2. Here, $\Delta\Sigma_h = (\Sigma_{xz}^{\Gamma} - \Sigma_{yz}^{\Gamma})/2$ denotes the nematic splitting at Γ and $\Delta\Sigma_e = (\Sigma_{yz}^{X} - \Sigma_{xz}^{Y})/2$ is the nematic splitting at $M = (X, Y)$ with $\Sigma_{yz/xz}^{\ell}$ being the *yz*/*xz* orbital component of the real part of the self-energy for the ℓ pocket (see Supplementary Note 1). The maximum values are chosen to match the experimental ones,[11,19–21] i.e., $\Delta\Sigma_{h/e} \simeq 15$ meV. The most dramatic changes due to the nematic order are found in the orbital occupation of the hole pocket (Fig. 2a, d). The presence of a relatively large spin–orbit coupling (≃20 meV) implies a mixing of the *xz* and *yz* orbitals on all the FS. However, below T_S the *yz* character of the hole pocket is strongly suppressed, and the pocket acquires a dominant *xz* character even at $\theta = 0$, as observed by the polarization dependent ARPES measurements.[17,19,26,27] At the same time, the nematic splitting enhances the *yz* occupation at *X* (Fig. 2b, e), and suppresses the *xz* at *Y* (Fig. 2c, f). As a consequence, one easily understands that considering the orbital character of the SC order parameter is not enough to explain the observed gap hierarchy. In fact, on the *X* pocket the gap is maximum at $\theta = \pi/2$, where the band has strong *yz* character, while on the Γ pocket it is larger at $\theta = 0$, where a dominant *xz* character is found. The crucial ingredient required to account for the SC properties of FeSe comes indeed from the nematic pairing provided by OSSF, as we show below.

By building up the spin-singlet vertex mediated by the SF, (6) and (7), one obtains (see Supplementary Note 2) a pairing Hamiltonian involving only the *xz*/*yz* orbital sector:

$$\begin{aligned} H_{\text{pair}}^{xz,yz} = & -g_X \sum_{\mathbf{k},\mathbf{k}'} u_{\Gamma,\mathbf{k}}^2 h_{\mathbf{k}}^{\dagger} h_{-\mathbf{k}}^{\dagger} u_{X,\mathbf{k}'}^2 e_{X,-\mathbf{k}'} e_{X,\mathbf{k}'} \\ & -g_Y \sum_{k,\mathbf{k}'} v_{\Gamma,\mathbf{k}}^2 h_{\mathbf{k}}^{\dagger} h_{-\mathbf{k}}^{\dagger} u_{Y,\mathbf{k}'}^2 e_{Y,-\mathbf{k}'} e_{Y,\mathbf{k}'} + h.c. \end{aligned} \tag{8}$$

The coefficients $u_{\ell,\mathbf{k}}$, $v_{\ell,\mathbf{k}}$, accounting for the pockets orbital character, preserve the C_4 band-structure symmetry above T_S and reproduce the nematic reconstruction below T_S. The $g_{X/Y}$ couplings control the strength of the pair hopping between the Γ and *X*/*Y* pockets. Within a spin-nematic scenario, OSSF below T_S are

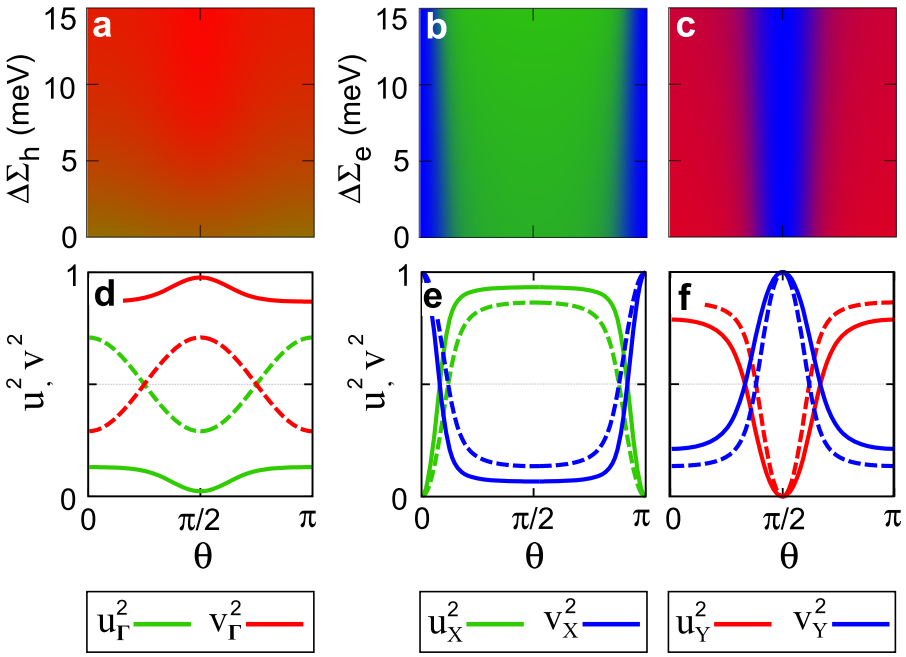

Fig. 2 Orbital content of the FS. **a**–**c** Color maps of the orbital content of the Γ (**a**), X (**b**), Y (**c**) pockets FS as a function of the angle and of the nematic splitting $\Delta\Sigma_{h/e}$. The color code is the same as in Fig. 1. **d**–**f** Orbital content of the same pockets as a function of θ at $\Delta\Sigma_{h/e}=0$, i.e., in the tetragonal phase (dashed lines) and in the nematic phase $\Delta\Sigma_{h/e}=15$ meV (solid lines)

stronger along Γ*X* than along Γ*Y* leading to a *nematic pairing anisotropy* with $g_X > g_Y$. Within the present itinerant-fermions picture, the SF are peaked at the wavevectors connecting hole-like with electron-like pockets. Thus, due to the absence in FeSe of the hole-like *xy* band at Γ one can neglect the spin-mediated pairing in the *xy* channel. However, SF at RPA level was found[31] to be most prominent at $\mathbf{Q}=(\pi,\pi)$. While this could be consistent with inelastic neutron scattering measurements at high temperatures, it does not account for the predominance of stripe-like SF at $(\pi, 0)$ in the nematic phase.[7] In addition, a predominant $\mathbf{Q}=(\pi,\pi)$ pairing channel implies a maximum gap value on the *xy* sector of the electron pocket, that is in sharp contrast with the experiments. This led the authors of refs. [22,31] to phenomenologically introduce orbital-dependent spectral weights to suppress this channel (see Discussion section). In general, one can still expect that a smaller pair hopping between the *X*, *Y* pockets is present in the *xy* sector. For the sake of completeness, and with the aim of reducing the number of free parameters, we considered also in this case only an interband *xy* pairing term, acting between the two electron-like pockets:

$$H^{xy}_{\rm pair} = -g_{xy}\sum_{\mathbf{k},\mathbf{k}\prime} v^2_{X,\mathbf{k}} e^\dagger_{X,\mathbf{k}} e^\dagger_{X,-\mathbf{k}} v^2_{Y,\mathbf{k}\prime} e_{Y,-\mathbf{k}\prime} e_{Y,\mathbf{k}\prime} + h.c. \tag{9}$$

The set of Eqs. (8) and (9) is solved in the mean-field approximation by defining the orbital-dependent SC order parameters for the hole $(\Delta^{yz}_h, \Delta^{xz}_h)$ and electron $(\Delta^{yz}_e, \Delta^{xz}_e, \Delta^{xy}_X, \Delta^{xy}_Y)$ pockets. The self-consistent equations at $T=0$ reads:

$$\Delta^{yz}_h = -g_X \sum_{\mathbf{k}} u^2_{X,\mathbf{k}}(u^2_{X,\mathbf{k}}\Delta^{yz}_e + v^2_{X,\mathbf{k}}\Delta^{xy}_X)/E_{X,\mathbf{k}} \tag{10}$$

$$\Delta^{xz}_h = -g_Y \sum_{\mathbf{k}} u^2_{Y,\mathbf{k}}(u^2_{Y,\mathbf{k}}\Delta^{xz}_e + v^2_{Y,\mathbf{k}}\Delta^{xy}_Y)/E_{Y,\mathbf{k}} \tag{11}$$

$$\Delta^{yz}_e = -g_X \sum_{\mathbf{k}} u^2_{\Gamma,\mathbf{k}}(u^2_{\Gamma,\mathbf{k}}\Delta^{yz}_h + v^2_{\Gamma,\mathbf{k}}\Delta^{xz}_h)/E_{\Gamma,\mathbf{k}} \tag{12}$$

$$\Delta^{xz}_e = -g_Y \sum_{k} v^2_{\Gamma,\mathbf{k}}(u^2_{\Gamma,\mathbf{k}}\Delta^{yz}_h + v^2_{\Gamma,\mathbf{k}}\Delta^{xz}_h)/E_{\Gamma,\mathbf{k}}, \tag{13}$$

$$\Delta^{xy}_X = -g_{xy} \sum_{\mathbf{k}} v^2_{Y,\mathbf{k}}(u^2_{Y,\mathbf{k}}\Delta^{xz}_e + v^2_{Y,\mathbf{k}}\Delta^{xy}_Y)/E_{Y,\mathbf{k}} \tag{14}$$

$$\Delta^{xy}_Y = -g_{xy} \sum_{\mathbf{k}} v^2_{X,\mathbf{k}}(u^2_{X,\mathbf{k}}\Delta^{xz}_e + v^2_{X,\mathbf{k}}\Delta^{xy}_X)/E_{X,\mathbf{k}} \tag{15}$$

Here, $E_{\ell,\mathbf{k}} = \sqrt{\varepsilon^2_{\ell,\mathbf{k}} + \Delta^2_{\ell,\mathbf{k}}}$ is the dispersion in the SC state, where $\varepsilon_{\ell,\mathbf{k}}$ is the band dispersion on each pocket $\ell = \Gamma, X, Y$ above T_c and $\Delta_{\ell,\mathbf{k}}$ is the band gap defined as:

$$\Delta_{\Gamma,\mathbf{k}} = u^2_{\Gamma,\mathbf{k}}\Delta^{yz}_h + v^2_{\Gamma,\mathbf{k}}\Delta^{xz}_h, \tag{16}$$

$$\Delta_{X,\mathbf{k}} = u^2_{X,\mathbf{k}}\Delta^{yz}_e + v^2_{X,\mathbf{k}}\Delta^{xy}_X, \tag{17}$$

$$\Delta_{Y,\mathbf{k}} = u^2_{Y,\mathbf{k}}\Delta^{xz}_e + v^2_{Y,\mathbf{k}}\Delta^{xy}_Y. \tag{18}$$

Superconducting gaps anisotropy

The overall momentum dependence of the band gaps is determined by the interplay between the momentum dependence of the orbital factors and the hierarchy of the orbital SC order parameters. In the absence of nematic order, Eqs. (10)–(18)

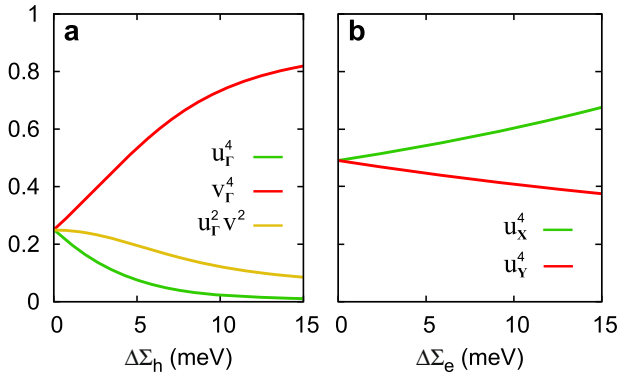

Fig. 3 Angular-averaged orbital-weight overlaps. **a**, **b** Nematic-splitting dependence of the angular-averaged orbital-weight overlaps appearing in the SC gap equations, i.e., Eqs. (10)–(13)

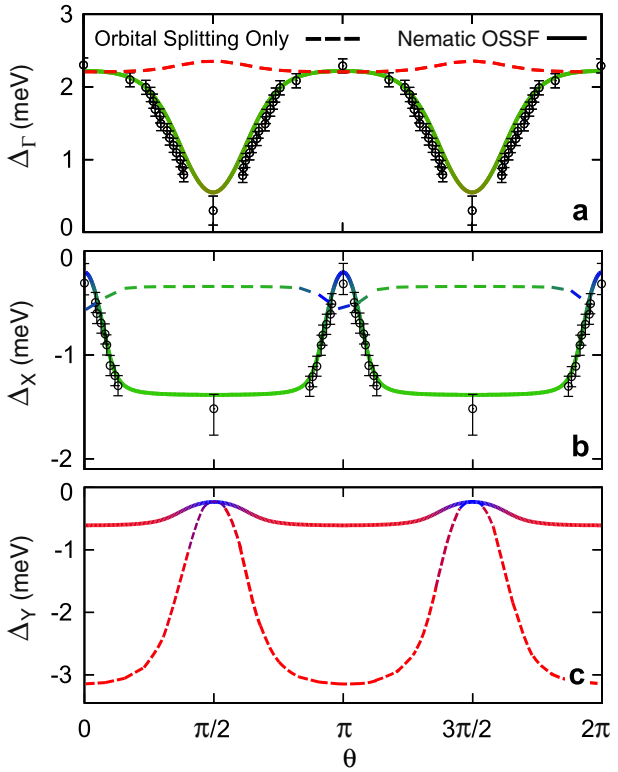

Fig. 4 Angular dependence of the SC band gaps. **a** SC gap on the hole, **b** on the *X* electron pocket, **c** on the *Y* electron pocket. Dashed lines are the results for the isotropic pairing $g_X/g_Y = 1$, while solid line for nematic pairing $g_X/g_Y \sim 21$. The color code accounts for the orbital component of the SC gap (green *yz*, red *xz*, blue *xy*), given by the product of the SC orbital parameter and the orbital weight, according to the definitions (16)–(18). For comparison, we reproduce the experimental gap values with standard deviations from ref. [22] (black circles)

preserve the symmetry in the exchange of the *xz*/*yz* orbitals. Thus, $\Delta_h^{xz} = \Delta_h^{yz}$ and the gap on the Γ pocket, Eq. (16), is constant, since $u_{\Gamma,\mathbf{k}}^2 + v_{\Gamma,\mathbf{k}}^2 = 1$. In the nematic state, the band structure breaks the C_4 symmetry, making $v_{\Gamma,\mathbf{k}}^2 \gg u_{\Gamma,\mathbf{k}}^2$ (see Fig. 2d), and also the SC orbital parameters Δ_h^{xz} and Δ_h^{yz} are in general different. However, as we shall see below, for isotropic pairing $g_X = g_Y$, the gaps anisotropy is the wrong one. The experimentally-observed anisotropy can only be achieved making $\Delta_{yz}^h \gg \Delta_{xz}^h$, that follows from the nematic pairing mechanism $g_X > g_Y$ provided by spin-nematic OSSF.

To understand the effect of the band-structure nematic reconstruction on the SC gap anisotropy, we show in Fig. 3 the evolution of the orbital-factors overlaps appearing in Eqs. (10)–(13), where we define the angular average of a given function as $\langle f(\mathbf{k})\rangle \equiv \int d\theta/(2\pi) f(k_F(\theta))$, with $k_F(\theta)$ FS wavevector of a given pocket. We can in first approximation neglect the pairing in the subleading *xy* channel and consider only what happens in the *xz*/*yz* orbital sector. As mentioned above, the nematic splitting on the electron pockets leads to a moderate enhancement of the *yz* factor appearing in Eq. (10) with respect to the *xz* in Eq. (11), i.e., $\langle u_X^4\rangle gt; rsim \langle u_Y^4\rangle$, Fig. 3b. This effect, recently highlighted while discussing the $k_z = \pi$ FS cut,[35] is however too small to account for the observed hole–gap anisotropy at $k_z = 0$. In fact, the strong modification of the hole-pocket orbital factors implies that $\langle u_\Gamma^4\rangle \ll \langle u_\Gamma^2 v_\Gamma^2\rangle < \langle v_\Gamma^4\rangle$, Fig. 3a. Thus, by neglecting logarithmic corrections in the gap ratios, from Eqs. (10)–(13) one obtains that

$$\frac{\Delta_e^{yz}}{\Delta_e^{xz}} \simeq \frac{g_X}{g_Y}\frac{\langle u_\Gamma^2 v_\Gamma^2\rangle}{\langle v_\Gamma^4\rangle} \simeq 0.1\frac{g_X}{g_Y} \tag{19}$$

and

$$\frac{\Delta_h^{yz}}{\Delta_h^{xz}} \simeq \frac{g_X}{g_Y}\frac{\langle u_X^4\rangle}{\langle u_Y^4\rangle}\frac{\Delta_e^{yz}}{\Delta_e^{xz}} \simeq 1.8\frac{g_X}{g_Y}\frac{\Delta_e^{yz}}{\Delta_e^{xz}}. \tag{20}$$

Note that Eqs. (19) and (20) are almost unaffected once the *xy* pairing channel is taken into account. From Eqs. (19) and (20), it follows that an isotropic pairing interaction $g_X = g_Y$ (as considered in ref. [35]) would lead to a suppression of the *yz* gap parameters. At the Γ pocket, where the *yz* orbital character is also strongly suppressed by nematicity ($u_\Gamma^2 \ll v_\Gamma^2$, Fig. 3a), the band gap would have only *xz* character, $\Delta_{\Gamma,\mathbf{k}} \simeq \Delta_h^{xz} v_{\Gamma,\mathbf{k}}^2$, leading to a small modulation with a relative maximum at $\theta = \pi/2$ (dashed line in Fig. 3a), in contrast with the experimental findings. On the other hand, the OSSF-mediated anisotropic pairing with $g_X/g_Y \gg 1$ gives a substantial *enhancement* of the $\Delta_h^{yz}/\Delta_h^{xz}$ ratio. This leads to $\Delta_{\Gamma,\mathbf{k}} \simeq \Delta_h^{yz} u_{\Gamma,\mathbf{k}}^2$, in agreement with the band-gap anisotropy observed experimentally as shown in Fig. 4a, where the numerical solutions of Eqs. (10)–(13) are reported along with the experimental data of ref. [22]. Here the color code does not refer to the orbital content of the pocket, as in Fig. 1, but to the orbital content of the SC gap function, that is determined by the product of the SC order parameter times the orbital weight in each sector, Eqs. (16)–(18).

The anisotropy $g_X/g_Y = 21$ extracted from this analysis is rather large, since one needs to overcome the strong suppression of the *yz* orbital due to nematic reconstruction at the hole pocket: one needs at least $g_X/g_Y \geq 2$ (not shown) to start to see the correct symmetry of the gap at Γ, i.e., a maximum at $\theta = 0$. The value of g_X/g_Y obtained by the SC-gaps analysis is compatible with the anisotropy of the OSSF used to reproduce the orbital-selective shrinking of the FS in the nematic phase[19] as discussed in Supplementary Note 3. In principle, the nematic-pairing anisotropy could also be estimated by the direct measurements of the SF. However, while it has been established that in the nematic phase SF are stronger at $(\pi, 0)$ than at (π, π),[6–8] the different intensity expected at $(\pi, 0)$ and $(0, \pi)$ has not been measured yet in detwinned samples.

The gap obtained for the *X* pocket is shown in Fig. 4b. Its value is also in overall in agreement with the Scanning Tunneling Microscopy (STM) experimental data.[22] To reproduce the experimental value of the *xy* component, we needed a small $(|g_{xy}| \ll g_X)$ attractive interband interaction between the two electron-like pockets. In fact, a negative g_{xy} guarantees, from Eqs. (14) and (15), that the SC *xy* order parameters on both electron pockets have the opposite sign with respect to the one at the hole pockets, as required by the dominant spin-mediated channel. In contrast, a repulsive g_{xy} induces a frustration that turns out in a gap with nodes along the FS.[41] Even though this has been

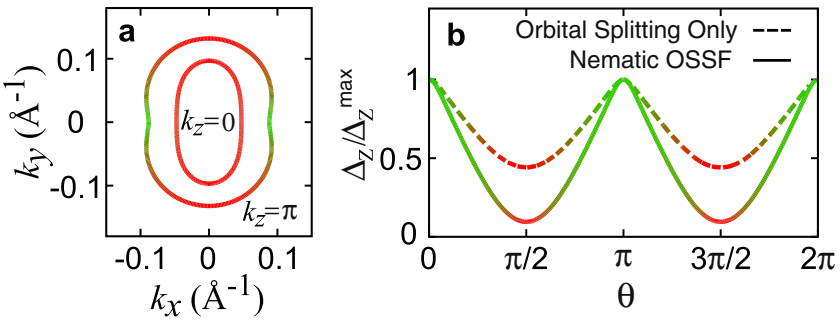

Fig. 5 FS and SC gap for the hole pocket at $k_z = \pi$. **a** FS at $k_z = 0$ and $k_z = \pi$ in the nematic phase. At $k_z = \pi$ the hole pocket retains a full *yz* orbital character at $\theta = 0$. **b** Angular dependence of the SC gap Δ_Z renormalized to its maximum value obtained using the same g_X/g_Y value extracted from the $k_z = 0$ gap fit (see Supplementary Note 3). Same color code of Fig. 4. The Δ_Z maximum at $\theta = 0$ is obtained already for isotropic pairing $g_X = g_Y$ (dashed lines), see also ref. [35]. The nematic pairing (solid lines) further enhances the gap anisotropy, leading to larger relative variations on the *Z* pocket, in agreement with ARPES experiments[28]

recently suggested by specific-heat measurements,[42] the STM data[22] shown for comparison exclude the presence of nodes and force us to consider a negative g_{xy}. It is important to stress that, even though the full set of Eqs. (10)–(15) must be solved self-consistently, adding or not the *xy* channel is not relevant for what concerns the understanding of the gap behavior in the *xz*/*yz* sector, especially for the gap anisotropy at the Γ pocket. For the sake of completeness, we report in Fig. 4c also the gap on the *Y* pocket, that has not been resolved so far in STM.[22] As one can see, for the electronic pockets an isotropic pairing $g_X = g_Y$ would lead to a strong difference between the absolute gap values at *X* and *Y*, due to the effect of nematic ordering at the electronic pockets, as one understands from Eq. (19) above. In contrast, nematic pairing leads to more similar gap values, which can be hardly disentangled experimentally, explaining why recent ARPES results claiming to resolve the *Y* pocket do not report appreciable significant gap differences on the two electron pockets.[28] The differences between the *X* and *Y* gaps due to the nematic pairing could however have implications for the thermal probes sensible to single-particle excitations. We leave the analysis of those effects for future work.

Recently, the k_z-dependence of the gap anisotropy on the hole pocket has been investigated,[28] and it has been shown that the $\Delta_\Gamma(\theta = 0)/\Delta_\Gamma(\theta = \pi/2)$ anisotropy increases as one moves from the $k_z = 0$ to the $k_z = \pi$ cut. Even though we did not consider a full 3D model, this effect can be understood by considering the variations of the hole-pocket orbital content when moving from $k_z = 0$ to $k_z = \pi$ (*Z* point). The larger size of the hole pocket at *Z* makes its orbital content less sensitive to nematic ordering and spin–orbit mixing, so that it still preserves a marked *yz* character around $\theta = 0$ (refs. [24,25,35]), with $u_\Gamma \sim cos\theta$ and $v_\Gamma \sim \sin\theta$ also in the nematic phase (Fig. 5a). In this situation, $\langle u_\Gamma^4 \rangle \sim \langle v_\Gamma^4 \rangle$ so that the enhancement $\langle u_X^4 \rangle > \langle u_Y^4 \rangle$ of the orbital factors in the electron pockets is enough to guarantee that $\Delta_h^{yz} > \Delta_h^{xz}$, leading to a hole-pocket gap anisotropy compatible with the measurements even when $g_X = g_Y$, as recently shown in ref. [35] (dashed line Fig. 5b). On the other hand, by retaining the same ratio g_X/g_Y value extracted from the $k_z = 0$ gap fit (solid line Fig. 5b), we find an increase of the anisotropy when moving from the Γ to the *Z* pocket. While this is consistent with the observations in pure[28] and S-doped[24] FeSe, other groups[25,26] report instead an overall smaller gap at $k_z = 0$. The analysis of SC fluctuations above T_c, could provide an alternative experimental test to clarify the 3D behavior. As shown in ref. [43], the crossover from 2D to 3D character of the fluctuation contribution to the paraconductivity is controlled by the k_z dependence of the pairing interactions. This effect, used to explain the measurements in 122 systems,[44] could be tested in FeSe as well.

DISCUSSION

The C_4 symmetry breaking of paramagnetic SF is a consequence of SF interactions beyond RPA.[32,34] As a consequence, the effects of the nematic SF pairing $g_X > g_Y$ highlighted in the present work cannot be captured by microscopic models where the SF are described at RPA level, even when RPA fluctuations are computed using the nematic reconstruction of the band structure.[31,45] An alternative route followed in refs. [22,31] amounts to start from band dispersions fitted to ARPES data and to account phenomenologically for the role of correlations. The so-called orbital differentiation of the electronic mass renormalization due to local electronic interactions has been studied in DMFT-like calculations in the tetragonal phase,[46,47] which found in particular a larger renormalization of the *xy* orbital with respect to the *xz*/*yz* ones. In addition, correlations can also cooperate to enhance the *xz*/*yz* orbital differentiation induced by other nematic mechanisms.[48] Inspired by these results, the authors of refs. [22,31] added phenomenologically orbital-dependent quasiparticle spectral weights, Z_{orb}, in the RPA-based calculation of the pairing interaction. By using $Z_{xy} \ll Z_{xz} < Z_{yz}$, they obtain the twofold result to make the *Y* pocket incoherent, explaining why it does not show up in the STM analysis,[22,49] and to move the maximum of SF from $\mathbf{Q} = (\pi, \pi)$ to $\mathbf{Q} = \mathbf{Q}_X$,[45] explaining the neutron-scattering experiments[7,8] and the observed gap hierarchy. However, this approach presents some inconsistencies. One issue is methodological: by using independent parameters to renormalize the band structure (that is fitted from the experiments) and to define the residua of the Green's functions, one misses the strict relation between these two quantities. On the other hand, by implementing this relation self-consistently, as done for example in ref. [50], it is not obvious how one can reconcile the large Fermi-velocity anisotropy implicit in the $Z_{xz} < Z_{yz}$ relation with the experimental band structure, that is well reproduced accounting only for a crystal-field splitting of the tetragonal band structure having $Z_{xz} = Z_{yz}$.[11,26,27] A second issue arises by the comparison with experiments. The route followed in refs. [22,31] is equivalent to rewrite the SC gap, e.g., on the Γ pocket as:

$$\Delta_{\Gamma,\mathbf{k}} = Z_{yz} u_{\Gamma,\mathbf{k}}^2 \Delta_h^{yz} + Z_{xz} v_{\Gamma,\mathbf{k}}^2 \Delta_h^{xz} \tag{21}$$

In our case, Eq. (16), the predominance of the SC *yz* orbital component is achieved via $\Delta_{yz}^h \gg \Delta_{xz}^h$, as guaranteed by the nematic-pairing condition $g_X \gg g_Y$. Instead in Eq. (21) this is mainly due to the rescaling of the orbital occupation factors by the corresponding spectral weights $Z_{yz/xz}$. By assuming $Z_{yz} \gg Z_{xz}$[22,31] one finds $\Delta_{\Gamma,\mathbf{k}} \approx Z_{yz} u_{\Gamma,\mathbf{k}}^2 \Delta_h^{yz}$, consistently with the measured gap anisotropy. However, the rescaling of the *yz* orbital occupation to $Z_{yz} u_{\Gamma,\mathbf{k}}^2$ is operative not only on the SC gap function, but also on the band structure above T_c. This restores the *yz*

character of the Γ pocket,[45] in contrast with ARPES measurements which clearly indicate[26,27] its predominant *xz* character.

To reconcile ARPES with RPA-based calculations of the spin-mediated pairing interactions, the authors of ref. [26] use the alternative approach to remove intentionally the contribution of the *Y* pocket from the RPA-mediated pairing interaction. This is equivalent to put $g_Y = 0$ in Eqs. (10)–(13), so that $\Delta_h^{xz} = 0$ and the modulation of the gap at Γ follows again the *yz* orbital weight, even if it is largely subdominant. With respect to these approaches, the main advantage of our model is to provide, via the orbital selectivity of the OSSF, a mechanism able to achieve the $g_X > g_Y$ nematic pairing without affecting strongly the quasiparticle spectral weights, while the main disadvantage is the lack of a theoretical justification for the missing *Y* pocket. However, we cannot help noticing that this point is also controversial from the experimental point of view, due to different reports claiming to observe[19,28] or not[22,26] the *Y* pocket.

In summary, our work provides a paradigm for the emergence of superconductivity in FeSe from an orbital-selective nematic SF mechanism. By combining the orbital ordering induced by the nematic shrinking of the FS pockets below the nematic transition with the anisotropic pairing interaction mediated by nematic SF, we explain the gap hierarchy reported experimentally on hole and electron pockets, and its variation with k_z. Our findings also offer a fresh perspective on previous attempts to explain the SC properties of FeSe, highlighting from one side the crucial role of spin-mediated pairing, and from the other side clarifying the importance of spin–spin interactions beyond RPA level. This result then represents a serious challenge for a full microscopic approach, that must account self-consistently for the emergence of Ising-nematic SF below the nematic transition temperature.

METHODS

Pairing by orbital-selective spin fluctuations

The mean-field equations for the pairing Hamiltonian, Eqs. (8) and (9), can be easily derived by defining the orbital-dependent SC order parameters for the hole $(\Delta_h^{yz}, \Delta_h^{xz})$ and electron $(\Delta_e^{yz}, \Delta_e^{xz})$ pockets as:

$$\Delta_e^{yz} = -g_X \langle u_{\Gamma,\mathbf{k}}^2 h_{\mathbf{k}} h_{-\mathbf{k}} \rangle, \tag{22}$$

$$\Delta_e^{xz} = -g_Y \langle v_{\Gamma,\mathbf{k}}^2 h_{\mathbf{k}} h_{-\mathbf{k}} \rangle, \tag{23}$$

$$\Delta_h^{yz} = -g_X \langle u_{X,\mathbf{k}}^2 e_{X,\mathbf{k}} e_{X,-\mathbf{k}} \rangle, \tag{24}$$

$$\Delta_h^{xz} = -g_Y \langle u_{Y,\mathbf{k}}^2 e_{Y,\mathbf{k}} e_{Y,-\mathbf{k}} \rangle, \tag{25}$$

$$\Delta_X^{xy} = -g_{xy} \langle v_{Y,\mathbf{k}}^2 e_{Y,\mathbf{k}} e_{Y,-\mathbf{k}} \rangle, \tag{26}$$

$$\Delta_Y^{xy} = -g_{xy} \langle v_{x,\mathbf{k}}^2 e_{X,\mathbf{k}} e_{X,-\mathbf{k}} \rangle, \tag{27}$$

The corresponding self-consistent BCS equations at $T = 0$ are the ones reported in the text, Eqs. (10)–(15). To solve them, we introduce polar coordinates and we approximate the orbital factors and the density of states with their values at the Fermi level for each pocket. This implies that the various integrals can be computed as for example:

$$\begin{aligned} \sum_{\mathbf{k}} u_{X,\mathbf{k}}^2 \frac{\Delta_{X,\mathbf{k}}}{E_{X,\mathbf{k}}} &= \int \frac{kdkd\theta}{(2\pi)^2} u_X^2(\theta) \frac{\Delta_X(\theta)}{\sqrt{\varepsilon_{X,\mathbf{k}}^2 + \Delta_X^2(\theta)}} \\ &= \int \frac{d\varepsilon d\theta}{(2\pi)} N_X(\varepsilon_F, \theta) u_X^2(\theta) \frac{\Delta_X(\theta)}{\sqrt{\varepsilon^2 + \Delta_X^2(\theta)}} \\ &= \int \frac{d\varepsilon d\theta}{(2\pi)} N_X(\varepsilon_F, \theta) u_X^2(\theta) \Delta_X(\theta) \log \frac{\omega_D}{\Delta_X(\theta)} \end{aligned} \tag{28}$$

where we defined $u_X^4(\theta) \equiv u_X^4(k_F(\theta))$ and $\Delta_X(\theta) \equiv \Delta_e^{yz} u_X^2(\theta) + \Delta_X^{xy} v_X^2(\theta)$. The cut-off ω_D represents the range of the spin-mediated pairing interaction, and it has been taken of order of 0.1 eV. The angular-dependent density of state is defined as usual as $N_X(\varepsilon_F, \theta) = \int (kdk)/(2\pi) \delta(\varepsilon_F - \varepsilon_{X,\mathbf{k}}) = k_F(\theta)/2\pi |v_F(\theta)|$, where $k_F(\theta)$ and $v_F(\theta)$ are the wavevector and velocity at the Fermi level, respectively. For a parabolic band dispersion, $N_X(\varepsilon_F, \theta)$ reduces to an angular-independent constant. Even though in Eq. (28) the angular integration involves both the orbital factor and the density of states, we checked that the results do not change considerably if the angular-averaged density of states is taken outside the integral. For this reason, accounting separately for the angular averages of the orbital factors alone, as shown in Fig. 3, allows one to have a rough estimate of the numerical results, as discussed in the text. The results of the full numerical self-consistent calculations of Eqs. (10)–(13) are displayed in Figs. 4 and 5 for $g_X/g_Y = 21$ and $|g_{xy}|/g_X = 0.076$. The numerical values of the band parameters can be found in Supplementary Note 3.

DATA AVAILABILITY

The authors declare that the data supporting the findings of this study are available within the paper and its supplementary notes.

ACKNOWLEDGEMENTS

We acknowledge M. Capone, A. Chubukov, and P. Hirschfeld for useful discussions; and M. Capone for critical reading of the manuscript. We acknowledge financial support by Italian MAECI under the collaborative Italia-India project SuperTop-PGR04879, by MINECO (Spain) via Grants No. FIS2014-53219-P and by Fundación Ramon Areces. We acknowledge the cost action Nanocohybri CA16218.

AUTHOR CONTRIBUTIONS

L.F. conceived the project with inputs from all coauthors. L.F. and L.B. performed the numerical calculations. All the authors contributed to the data analysis, to the interpretation of the theoretical results, and to the writing of the text.

ADDITIONAL INFORMATION

Supplementary information accompanies the paper on the *npj Quantum Materials* website (https://doi.org/10.1038/s41535-018-0129-9).

Competing interests: The authors declare no competing interests.

Publisher's note: Springer Nature remains neutral with regard to jurisdictional claims in published maps and institutional affiliations.

REFERENCES

1. Mazin, I. I., Singh, D. J., Johannes, M. D. & Du, M. H. Unconventional superconductivity with a sign reversal in the order parameter of $LaFeAsO_{1-x}F_x$. *Phys. Rev. Lett.* **101**, 057003 (2008).
2. Kuroki, K. et al. Unconventional pairing originating from the disconnected Fermi surfaces of superconducting $LaFeAsO_{1-x}F_x$. *Phys. Rev. Lett.* **101**, 087004 (2008).
3. Chubukov, A. Pairing mechanism in Fe-based superconductors. *Annu. Rev. Condens. Matter Phys.* **3**, 57–92 (2012).
4. Platt, C., Hanke, W. & Thomale, R. Functional renormalization group for multi-orbital Fermi surface instabilities. *Adv. Phys.* **62**, 453–562 (2013).
5. Hirschfeld, P. J. Using gap symmetry and structure to reveal the pairing mechanism in Fe-based superconductors. *C. R. Phys.* **17**, 197–231 (2016).
6. Rahn, M. C., Ewings, R. A., Sedlmaier, S. J., Clarke, S. J. & Boothroyd, A. T. Strong (π,0) spin fluctuations in β-FeSe observed by neutron spectroscopy. *Phys. Rev. B* **91**, 180501 (2015).
7. Wang, Q. et al. Strong interplay between stripe spin fluctuations, nematicity and superconductivity in FeSe. *Nat. Mater.* **15**, 159 (2016).
8. Wang, Q. et al. Magnetic ground state of FeSe. *Nat. Commun.* **7**, 12182 (2016).
9. He, M. et al. Evidence for short-range magnetic order in the nematic phase of FeSe from anisotropic in-plane magnetostriction and susceptibility measurements. *Phys. Rev. B* **97**, 104107 (2018).
10. Wiecki, P. et al. Persistent correlation between superconductivity and antiferromagnetic fluctuations near a nematic quantum critical point in $FeSe_{1-x}S_x$. *Phys. Rev. B* **98**, 020507 (2018).
11. Coldea, A. I. & Watson, M. D. The key ingredients of the electronic structure of FeSe. *Annu. Rev. Condens. Matter Phys.* **9**, 125–146 (2018).
12. Gallais, Y. & Paul, I. Charge nematicity and electronic Raman scattering in iron-based superconductors. *C. R. Phys.* **17**, 113–139 (2016).
13. Shimojima, T. et al. Lifting of *xz*/*yz* orbital degeneracy at the structural transition in detwinned FeSe. *Phys. Rev. B* **90**, 121111 (2014).
14. Nakayama, K. et al. Reconstruction of band structure induced by electronic nematicity in an FeSe superconductor. *Phys. Rev. Lett.* **113**, 237001 (2014).
15. Watson, M. D. et al. Emergence of the nematic electronic state in FeSe. *Phys. Rev. B* **91**, 155106 (2015).

16. Zhang, P. et al. Observation of two distinct d_{xz}/d_{yz} band splittings in FeSe. *Phys. Rev. B* **91**, 214503 (2015).
17. Suzuki, Y. et al. Momentum-dependent sign inversion of orbital order in superconducting FeSe. *Phys. Rev. B* **92**, 205117 (2015).
18. Zhang, Y. et al. Distinctive orbital anisotropy observed in the nematic state of a FeSe thin film. *Phys. Rev. B* **94**, 115153 (2016).
19. Fanfarillo, L. et al. Orbital-dependent Fermi surface shrinking as a fingerprint of nematicity in FeSe. *Phys. Rev. B* **94**, 155138 (2016).
20. Fedorov, A. et al. Effect of nematic ordering on electronic structure of FeSe. *Sci. Rep.* **6**, 36834 (2016).
21. Watson, M. D., Haghighirad, A. A., Rhodes, L. C., Hoesch, M. & Kim, T. K. Electronic anisotropies revealed by detwinned angle-resolved photo-emission spectroscopy measurements of FeSe. *New J. Phys.* **19**, 103021 (2017).
22. Sprau, P. O. et al. Discovery of orbital-selective cooper pairing in FeSe. *Science* **357**, 75–80 (2017).
23. Song, C.-L. et al. Direct observation of nodes and twofold symmetry in FeSe superconductor. *Science* **332**, 1410–1413 (2011).
24. Xu, H. C. et al. Highly anisotropic and twofold symmetric superconducting gap in nematically ordered $FeSe_{0.93}S_{0.07}$. *Phys. Rev. Lett.* **117**, 157003 (2016).
25. Hashimoto, T. et al. Superconducting gap anisotropy sensitive to nematic domains in FeSe. *Nat. Commun.* **9**, 282 (2018).
26. Rhodes, L. C. et al. Scaling of the superconducting gap with orbital character in FeSe. Preprint at arXiv:1804.01436 (2018).
27. Liu, D. et al. Orbital origin of extremely anisotropic superconducting gap in nematic phase of FeSe superconductor. *Phys. Rev. X* **8**, 031033 (2018).
28. Kushnirenko, Y. S. et al. Three-dimensional superconducting gap in FeSe from angle-resolved photoemission spectroscopy. *Phys. Rev. B* **97**, 180501 (2018).
29. Sato, Y. et al. Abrupt change of the superconducting gap structure at the nematic critical point in $FeSe_{1-x}S_x$. *Proc. Natl. Acad. Sci. U.S.A.* **115**, 1227–1231 (2018).
30. Sun, Y. et al. Gap structure of FeSe determined by angle-resolved specific heat measurements in applied rotating magnetic field. *Phys. Rev. B* **96**, 220505 (2017).
31. Kreisel, A. et al. Orbital selective pairing and gap structures of iron-based superconductors. *Phys. Rev. B* **95**, 174504 (2017).
32. Fanfarillo, L., Benfatto, L. & Valenzuela, B. Orbital mismatch boosting nematic instability in iron-based superconductors. *Phys. Rev. B* **97**, 121109 (2018).
33. Fernandez-Martin, R., Fanfarillo, L., Benfatto, L. & Valenzuela, B. DC conductivity anisotropy by orbital selective spin fluctuations in the nematic phase of iron superconductors. Preprint at arXiv:1804.07293 (2018).
34. Fernandes, R., Chubukov, A. & Schmalian, J. What drives nematic order in iron-based superconductors? *Nat. Phys.* **10**, 97 (2014).
35. Kang, J., Fernandes, R. M. & Chubukov, A. Superconductivity in FeSe: the role of nematic order. *Phys. Rev. Lett.* **120**, 267001 (2018).
36. Cvetkovic, V. & Vafek, O. Space group symmetry, spin–orbit coupling, and the low-energy effective Hamiltonian for iron-based superconductors. *Phys. Rev. B* **88**, 134510 (2013).
37. Fanfarillo, L., Cortijo, A. & Valenzuela, B. Spin-orbital interplay and topology in the nematic phase of iron pnictides. *Phys. Rev. B* **91**, 214515 (2015).
38. Ortenzi, L., Cappelluti, E., Benfatto, L. & Pietronero, L. Fermi-surface shrinking and interband coupling in iron-based pnictides. *Phys. Rev. Lett.* **103**, 046404 (2009).
39. Coldea, A. I. et al. Fermi surface of superconducting LaFePO determined from quantum oscillations. *Phys. Rev. Lett.* **101**, 216402 (2008).
40. Brouet, V. et al. Large temperature dependence of the number of carriers in co-doped $BaFe_2As_2$. *Phys. Rev. Lett.* **110**, 167002 (2013).
41. Kemper, A. F. et al. Sensitivity of the superconducting state and magnetic susceptibility to key aspects of electronic structure in ferropnictides. *New J. Phys.* **12**, 073030 (2010).
42. Hardy, F. et al. Nodal gaps in the nematic superconductor FeSe from heat capacity. Preprint at arXiv:1807.07907 (2018).
43. Fanfarillo, L. & Benfatto, L. Anisotropy of the superconducting fluctuations in multiband superconductors: the case of LiFeAs. *Supercond. Sci. Technol.* **27**, 124009 (2014).
44. Rullier-Albenque, F., Colson, D., Forget, A. & Alloul, H. Multiorbital effects on the transport and the superconducting fluctuations in LiFeAs. *Phys. Rev. Lett.* **109**, 187005 (2012).
45. Kreisel, A., Andersen, B. M. & Hirschfeld, P. Itinerant approach to magnetic neutron scattering of FeSe: effect of orbital selectivity. Preprint at arXiv:1807.09482 (2018).
46. de'Medici, L., Georges, A. & Biermann, S. Orbital-selective mott transition in multiband systems: slave-spin representation and dynamical mean-field theory. *Phys. Rev. B* **72**, 205124 (2005).
47. de' Medici, L., Giovannetti, G. & Capone, M. Selective mott physics as a key to iron superconductors. *Phys. Rev. Lett.* **112**, 177001 (2014).
48. Fanfarillo, L., Giovannetti, G., Capone, M. & Bascones, E. Nematicity at the Hund's metal crossover in iron superconductors. *Phys. Rev. B* **95**, 144511 (2017).
49. Kostin, A. et al. Imaging orbital-selective quasiparticles in the hund's metal state of FeSe. *Nat. Mater.* **17**, 869–874 (2018).
50. Hu, H., Yu, R., Nica, E. M., Zhu, J.-X. & Si, Q. Orbital-selective superconductivity in the nematic phase of FeSe. Preprint at arXiv:1805.05915 (2018).